The Astrophysical Journal Letters, 849:L16 (7pp), 2017 November 1 https://doi.org/10.3847/2041-8213/aa9367

Distance and Properties of NGC 4993 as the Host Galaxy of the Gravitational-wave Source GW170817

Myungshin Im[1], Yongmin Yoon[1], Seong-Kook J. Lee[1], Hyung Mok Lee[2], Joonho Kim[1], Chung-Uk Lee[3], Seung-Lee Kim[3], Eleonora Troja[4,5], Changsu Choi[1], Gu Lim[1], Jongwan Ko[3], and Hyunjin Shim[6]
[1] Center of the Exploration of the Origin of the Universe, Astronomy Program, Department of Physics & Astronomy, Seoul National University, 1 Gwanak-rho, Gwanak-gu, Seoul 08826, Korea; mim@astro.snu.ac.kr
[2] Astronomy Program, Department of Physics & Astronomy, Seoul National University, 1 Gwanak-rho, Gwanak-gu, Seoul 08826, Korea
[3] Korea Astronomy and Space Science Institute, 776 Daedeokdae-ro, Yuseong-gu, Daejeon 34055, Korea
[4] Department of Astronomy, University of Maryland, College Park, MD 20742-4111, USA
[5] NASA Goddard Space Flight Center, 8800 Greenbelt Road, Greenbelt, MD 20771, USA
[6] Department of Earth Science Education, Kyungpook National University, 80 Daehak-ro, Buk-gu, Daegu 41566, Korea
Received 2017 October 2; revised 2017 October 10; accepted 2017 October 13; published 2017 October 26

Abstract

Recently, the optical counterpart of the gravitational-wave source GW170817 has been identified in the NGC 4993 galaxy. Together with evidence from observations in electromagnetic waves, the event has been suggested as a result of a merger of two neutron stars (NSs). We analyze the multi-wavelength data to characterize the host galaxy property and its distance to examine if the properties of NGC 4993 are consistent with this picture. Our analysis shows that NGC 4993 is a bulge-dominated galaxy with $r_{\rm eff} \sim$ 2–3 kpc and a Sérsic index of $n = 3$–4 for the bulge component. The spectral energy distribution from 0.15 to 24 μm indicates that this galaxy has no significant ongoing star formation, a mean stellar mass of (0.3–1.2) $\times$ 10^{11} $M_{\odot}$, a mean stellar age greater than ∼3 Gyr, and a metallicity of about 20%–100% of solar abundance. Optical images reveal dust lanes and extended features that suggest a past merging activity. Overall, NGC 4993 has characteristics of normal, but slightly disturbed elliptical galaxies. Furthermore, we derive the distance to NGC 4993 with the fundamental plane relation using 17 parameter sets of 7 different filters and the central stellar velocity dispersion from the literature, finding an angular diameter distance of 37.7 $\pm$ 8.7 Mpc. NGC 4993 is similar to some host galaxies of short gamma-ray bursts (GRBs) but much different from those of long GRBs, supporting the picture of GW170817 as a result of the merger of two NSs.

Key words: galaxies: elliptical and lenticular, cD – galaxies: fundamental parameters – galaxies: individual (NGC 4993) – gravitational waves

1. Introduction

Since 2015, the Advanced Laser Interferometer Gravitational-wave Observatory (LIGO) and the Advanced Virgo have succeeded in detecting a number of gravitational-wave (GW) signals coming from distant black hole (BH) merger events (Abbott et al. 2016, 2017a). However, the detected GW events so far have resulted from mergers of two stellar mass BHs that are unlikely to produce detectable optical signals, and no optical sources have been identified that correspond to the GW sources. A merger of two neutron stars (NSs) or an NS and a BH has been suggested as a GW source that produces an optical signal. Indeed, NS mergers are thought to be responsible for short gamma-ray bursts (GRBs) when viewed on-axis, and models have predicted an optical signal, known as a kilonova, to be produced in such an event when viewed off-axis (e.g., see a review by Metzger 2017 and references therein).

GW170817 is a GW source whose signal was detected by the Advanced LIGO and the Advanced Virgo on 2017 August 17, 12:41:04 UT (Abbott et al. 2017b). A weak and short (∼2 s) gamma-ray signal was caught by the *Fermi* Gamma-ray Space Telescope and *INTEGRAL* 2 s after the GW detection (Goldstein et al. 2017; Savchenko et al. 2017). The GW signal showed that this could be a merger of two NSs at a distance of 40^{+8}_{-14} Mpc (Abbott et al. 2017b). About 11 hr after the LIGO detection, an optical counterpart of the GW source was reported (Coutler et al. 2017) in a nearby galaxy, NGC 4993. The source has been found to have characteristics of off-axis short GRBs and a kilonova (e.g., Troja et al. 2017).

If GW170817 is caused by a binary NS (BNS) merger, the host galaxy is expected to have properties similar to the hosts of short GRBs. So far, host galaxies of short GRBs are known to have ages in the range of several tens of Myr to ∼5 Gyr, stellar masses of $10^{8.5-11.8}$ $M_{\odot}$ (a median value of 10^{10} $M_{\odot}$), a 0 to ∼10 $M_{\odot}$ $\rm yr^{-1}$ star formation rate, a median metallicity of solar abundance, and morphology of both spirals and ellipticals (Leibler & Berger 2010; Berger 2014; Troja et al. 2016). This is very different from hosts of long GRBs that are younger, actively star-forming, less metal-rich, and less massive (e.g., Michałowski et al. 2012).

The host galaxy, NGC 4993, is known as an early-type galaxy in the ESO 508 cluster. The distance to ESO 508 has been measured to be 41.1 Mpc using the Cepheid-calibrated Tully–Fisher relation on the cluster spiral galaxies (Sakai et al. 2000), but this is by no means a direct measurement of distance to NGC 4993. Furthermore, while analysis of the GW signal provides an independent measurement of the luminosity distance, the distance based on GWs can suffer from a non-negligible amount of uncertainties, mostly due to the uncertainties in the inclination angle of the orbital plane with respect to the line of sight (Abbott et al. 2016). If the distance is accurately measured by other means, the inclination angle of the orbital plane can be well constrained. In that sense, accurate measurements of the distances to the host galaxies are very important.

About 8 hr after the first identification of the optical counterpart, we started follow-up observation of GW170817 (M. Im et al. 2017, in preparation; Troja et al. 2017). The accumulated data set allows us to construct deep images that can unveil faint, extended features and to accurately determine physical parameters of NGC 4993. Using these images, as well as other multi-wavelength data, we study properties of NGC 4993 to examine if this galaxy has the characteristics of short GRB hosts and derive an independent measure of its distance. To obtain the physical sizes, we adopt the angular diameter distance of 37.7 Mpc from this Letter. The magnitudes are in the AB system.

2. Data

2.1. Korean Microlensing Telescope Network (KMTNet) and LSGT Observations

We observed NGC 4993 from 2017 August 18 through September 7 at three locations: the Siding Spring Observatory (SSO) in Australia, the South African Astronomical Observatory (SAAO) in South Africa, and the Cerro-Tololo Inter-American Observatory (CTIO) in Chile, using 1.6 m telescopes of the KMTNet (Kim et al. 2016). Images were taken in B, V, R, and I filters, and the data are reduced with the standard KMTNet pipeline. These data are stacked to create deep images with total integration times of 1140 s, 1260 s, 7760 s, and 9900 s for the B, V, R, and I filters respectively. The surface brightness (SB) limit reaches to 27.9 mag arcsec^{-2} in the R band (1σ) when the pixels[7] are binned 9×9. We calibrated the photometry using the AAVSO Photometric All-Sky Survey (APASS) stars within 30′ from NGC 4993 at a magnitude range of 14–17. When stacking images, we used background-subtracted images for which the flux scales are normalized. The background subtraction was carefully done by choosing a large background estimation kernel (10′ or larger) so that the background does not get oversubtracted during this process.

We also observed NGC 4993 using the SNUCAM-II (Choi & Im 2017) on the 0.43 m Lee Sang Gak Telescope (LSGT; Im et al. 2015) and 0.5 m class telescopes of the iTelescope.Net at SSO from 2017 August 18 through September 11. For the observation, we used the u, g, r, i, z, a set of medium-band filters, and B, V, R, I filters. The u-band image has one hour on-source integration, and it is used to derive the u-band flux for SED fitting. The photometry calibration was done by using the APASS and the Two Micron All Sky Survey (2MASS) data of stars near NGC 4993 as described in Choi & Im (2017).

2.2. Archive Data

The *GALEX* All-sky Imaging Survey observed NGC 4993 in far- and near-ultraviolet (FUV and NUV), and the stacked, calibrated images are taken from the *GALEX* data archive. Coadded g, r, i, z, and y filter images are obtained from the Panoramic Survey Telescope and Rapid Response System (Pan-STARRS) Data Release 1 (Chambers et al. 2016). We also used the publicly available F606W image taken by the *HST* Advanced Camera for Surveys (ACS). In the infrared, the J, H, and K_s filter images are taken from 2MASS, and we also utilized the *WISE* $W1$, $W2$, $W3$, and $W4$ images.

[7] KMTNet pixel scale is 0.″396.

3. Morphology and Structural Parameters

Figure 1 shows the stacked KMTNet R, the *HST* $F606W$, Pan-STARRS g, r, i color-composite, and *WISE* $W1$ band images. In the inner region of a scale of about 1 kpc, we see dust lanes and a nuclear part that appears to have a dust-obscuring central disk. At an outer region of 10 kpc scale, we find several layers of extended features that are commonly regarded as a remnant feature of past merger activities (Kim & Im 2013). Even further out, we find that the outermost part of the galaxy extends out to 2′ in radius (22 kpc or 8 times that of the angular effective radius $\theta_{\rm eff}$[8]), which is visible in both the 9×9 binned R-band image and the $W1$ image. This shows that special care must be taken when stacking images and fitting an SB profile, so that the extended low SB feature is not washed away.

We performed the two-dimensional SB fitting using the GALFIT software (Peng et al. 2010) on the B, V, R, I, $F606W$, J, H, and K_s images. The point-spread functions are constructed using stars in the vicinity of NGC 4993 in each band. Several models have been used, such as (i) a single-Sérsic component model; (ii) a two-component model with a Sérsic profile and an exponential profile; and (iii) a double-Sérsic component model. We also performed a growth curve analysis to derive $\theta_{\rm eff}$ of NGC 4993 independently.

The result of the two-dimensional SB fitting is summarized below and in Table 1. The three models can fit the observed SB profile almost equally well, with the two-component models at a slightly better $\chi^2_{\rm red}$ (e.g., $\chi^2_{\rm red} = 0.985$ (single) versus 0.962 (two-component)). However, the single-Sérsic component model returns $\theta_{\rm eff}$ values about 15% larger than the two-component models. The growth curve analysis of the KMTNet data agrees with the two-component model results, and we attribute the larger $\theta_{\rm eff}$ from the single-Sérsic models to an inherent nature of a single-Sérsic profile with a large n that tends to distribute its light to regions at $r \gg \theta_{\rm eff}$. Therefore, we show the result from the Sérsic + exponential profile model only. In the single-Sérsic model, the Sérsic index n is found to be 4–5, a value common for elliptical galaxies. With a Sérsic bulge + exponential disk model, we find $B/T \gtrsim 0.7$ with $n = 3.0$–4.4 for the Sérsic bulge. The derived $\theta_{\rm eff}$ values correspond to physical effective radii of $r_{\rm eff} = 2$–3 kpc.

4. Stellar Population

We fit the multi-band photometric data points from FUV to mid-infrared (MIR; up to $W2$) using the SED-fitting software of Lee et al. (2015 and references therein). This SED model utilizes the stellar population synthesis model of Bruzual & Charlot (2003), with Padova 1994 stellar evolutionary tracks, the Chabrier (2003) initial mass function with a stellar mass range of 0.1–100 $M_\odot$, and a star formation rate in the form of $\frac{t}{\tau^2}e^{-t/\tau}$, where t is time since the onset of the star formation and τ is the timescale parameter. To fit the data, we used the flux within an aperture of a 30″ diameter (5.5 kpc), which was chosen to avoid possible bias due to missing fluxes from the outer, low SB features in shallower images of some filters. The Galactic extinction was corrected by adopting $E(B-V) = 0.106$ based on the extinction map of Schlafly & Finkbeiner (2011) and the extinction curve with $R_V = 3.1$ of Fitzpatrick (1999). The procedure fits five parameters: age, τ, metallicity,

[8] This is a fitted parameter from the SB-fitting, converted to a circularized value based on the model fit.

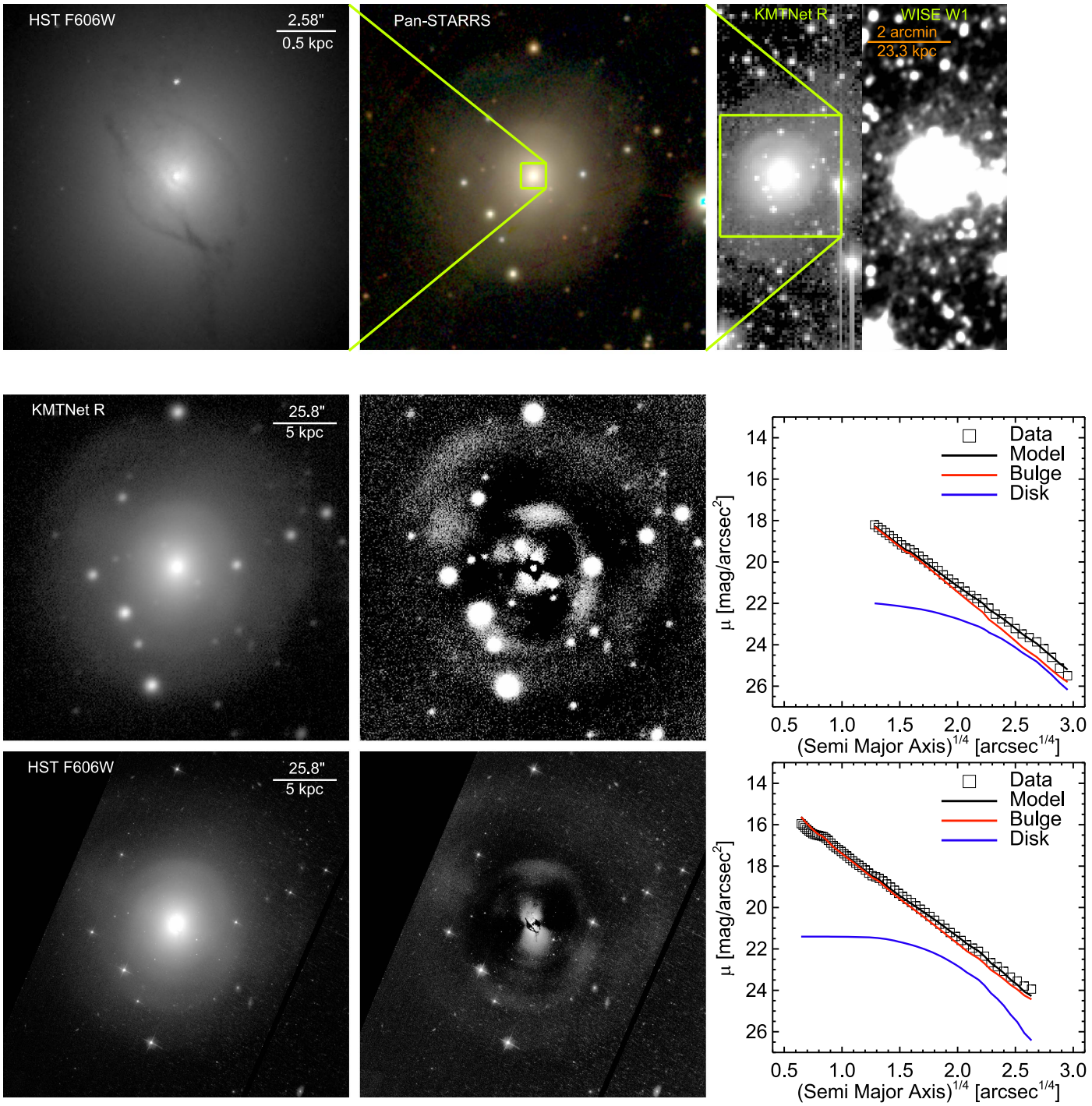

Figure 1. Images of NGC 4993 and the result of the SB fitting. The top panels show NGC 4993 in the innermost region (*HST F606W*), the region over several $\theta_{\rm eff}$ radii (the Pan-STARRS color composite), and the outer region that extends out to 8 $\theta_{\rm eff}$ radii (9 × 9 binned KMTNet *R*-band and *WISE W1* images). The *F606W* image reveals dust lanes in the inner part of NGC 4993, while the Pan-STARRS and the KMTNet images show extended features in the outer part. In the second and the third rows, we show the SB-fitting results for the *R* and the *F606W* images. From left to right, we show the original image, the residual image after the model image subtraction, and the one-dimensional SB profile of the best-fit model in comparison to the data. The one-dimensional SB profile shows that NGC 4993 has an SB with a Sérsic index around $n = 4$, a typical value for elliptical galaxies.

$E(B-V)$, and stellar mass. The best-fit stellar mass is scaled up by using the ratio of the total flux to the 30″ diameter aperture flux in the *H* band. There is a slight excess at 12 and 24 μm (*W3* and *W4*) over the stellar radiation. Therefore, we also tried to fit the SED with SSP model templates that include AGB dust emission (Piovan et al. 2003), and we added the *W3* and *W4* data points in the fitting. The fitting results are presented in Figure 2 and Table 2. Note that a similar result is also presented in Troja et al. (2017), but here we try the fitting with the updated data and include the AGB–dust emission model.

These SED-fitting results indicate that NGC 4993 has a stellar mass of (3–6) × 10^{10} $M_{\odot}$, a metallicity of 20% to 100% (with the best fit at 100%), and a τ of 0.3–0.5 Gyr. The age is loosely constrained to be $\gtrsim$3 Gyr (95% confidence). However, the stellar mass is sensitive to the assumed initial mass function

Table 1
SB-fitting Result

Filter	Inst.	Bulge mag (AB)	Bulge $\theta_{\rm eff}$[a] (arcsec)	n	Bulge b/a	Disk mag (AB)	Disk $\theta_{\rm eff}$[a] (arcsec)	Disk b/a	Total mag (AB)	Total $\theta_{\rm eff}$[a] (arcsec)	B/T	$\langle\mu\rangle_e$ (mag arcsec^{-2})
B	KMTNet	13.6	9.8	3.0	0.83	14.5	32.3	0.83	13.2	15.4	0.68	21.15
V	KMTNet	12.5	11.8	3.6	0.83	14.1	35.8	0.69	12.3	15.6	0.81	20.28
R	KMTNet	12.2	11.0	3.9	0.84	13.6	30.3	0.75	11.9	14.9	0.78	19.81
I	KMTNet	12.0	8.6	3.5	0.84	12.8	30.4	0.82	11.5	14.2	0.68	19.29
F606W	*HST* ACS	12.4	14.8	4.6	0.88	14.2	15.8	0.95	12.2	15.1	0.84	20.11
J	2MASS	11.3	7.9	4.3	0.79	12.3	22.1	0.84	10.9	12.0	0.72	18.32
H	2MASS	11.1	7.2	4.0	0.79	12.2	23.1	0.66	10.7	10.8	0.75	17.90
K	2MASS	11.0	9.2	4.4	0.82	13.7	21.0	0.14	10.9	10.3	0.92	18.03

Note. Apparent magnitudes and SBs are not corrected for the Galactic extinction.
[a] Circularized effective radii. To get the major axis value, multiply it by $\sqrt{a/b}$.

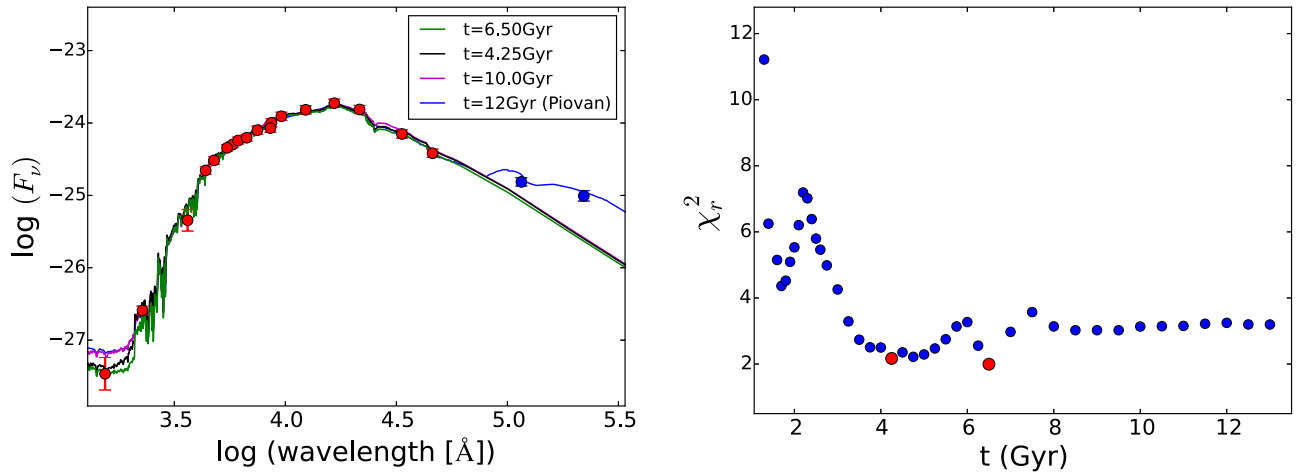

Figure 2. (Left) The broadband SED of NGC 4993 in *FUV*, *NUV*, u, g, r, i, z, y, B, V, R, I, J, H, K, $W1$, $W2$, $W3$, and $W4$. Overplotted are four SED models that provide a reasonably good match to the data points, among which the best-fit model is the model with $t = 6.5$ Gyr. The Piovan model includes the dust emission from AGB stars. (Right) The reduced χ^2 distribution as a function of the mean stellar age shows two local minima, and a long tail with a reasonably good fit at $t > 3$ Gyr.

(IMF). If we assume the Salpeter IMF instead, the stellar mass becomes about two times larger. Since both the Salpeter and the Chabrier IMFs are plausible (Capperllari et al. 2012), we conclude that NGC 4993 has a mean stellar mass in the range of $(0.3–1.2) \times 10^{11}\,M_\odot$. The star formation rate is very low, at a value of $\sim 4 \times 10^{-3}\,M_\odot\ \mathrm{yr}^{-1}$ or less, which is consistent with no star formation activity. A small amount of internal dust extinction ($E(B-V) = 0.025–0.075$) is consistent with the presence of the dust lanes.

The observed MIR excess at $>5\ \mu$m is common in early-type galaxies, and is possibly due to the dust emission from circumstellar materials around AGB stars (Shim et al. 2011; Ko et al. 2012), residual star formation, or active galactic nuclei (AGNs). We examine the *WISE* 12 and 24 μm images and find that the MIR light distribution is extended and follows the optical light distribution. Furthermore, the excess can be explained with a relatively old model that incorporates the AGB dust emission. On the other hand, the expected MIR flux from AGN activity as measured from the X-ray is two orders of magnitude lower than the excess value. Therefore, we suggest that the MIR excess is due to the dust emission from AGB circumstellar materials.

5. Distance

Early-type galaxies exhibit a tight correlation between $r_{\rm eff}$, the SB within $r_{\rm eff}$, $\langle\mu\rangle_e$, and the central velocity dispersion σ_0, known as the fundamental plane (FP) relation. Since $\langle\mu\rangle_e$ and σ_0 are quantities that can be measured without knowing distance, FP can be used to measure distances to early-type galaxies. The FP can be expressed as

$$\log(r_{\rm eff}\ h_{70}^{-1}/\mathrm{kpc}) = a\ \log(\sigma_0/\mathrm{km\ s^{-1}}) + b\ \langle\mu\rangle_e + c, \quad (1)$$

where the coefficients a, b, and c vary with wavelength (Jun & Im 2008; La Barbera et al. 2010).

Once $r_{\rm eff}$ is determined, the angular distance d_A is calculated as

$$d_A = (r_{\rm eff}\ h_{70}^{-1}/\mathrm{kpc}) \times \frac{206265}{\theta_{\rm eff}/\ \mathrm{arcsec}}. \quad (2)$$

We gathered four independent measurements of $\log(\sigma_0/\mathrm{km\ s^{-1}})$ from the literature: 2.312 ± 0.095 (Carter et al. 1988), 2.237 ± 0.013 (Beuing et al. 2002), 2.292 ± 0.042[9] (Wegner et al. 2003), and 2.212 ± 0.045 (Ogando et al. 2008). We adopt a weighted mean value, $\langle \log(\sigma_0/\mathrm{km\ s^{-1}})\rangle = 2.241 \pm 0.012$, of the four independent measurements. Using the $\langle\mu\rangle_e$ values from Table 1 after applying the Galactic extinction correction and the FP coefficients from various sources, we derive distances to NGC 4993 in seven different bands. Table 3 summarizes the result. In total, 17 different estimates are derived. Two of the FP relations are based on g, r, i, and z (Bernardi et al. 2003; La Barbera et al. 2010), and for these cases, the B, V, R, and I values are converted to g, r, and i values while keeping the structural parameters in the corresponding bands. Uncertainties in the distances are dominated by the intrinsic dispersion in the FP relation, which has errors of about 7 to 12 Mpc (or 23% of the derived value; e.g., Bernardi et al. 2003). The errors from the observed quantities amount to only $\lesssim$10% of the FP distance, and we ignore them. The uncertainty in the Hubble constant is only a few percent or less according to recent estimates (e.g., Riess et al. 2016) and also can be neglected. We note that the rms dispersion of the 17 estimates is 5.3 Mpc, smaller than the FP distance error of each estimate. This suggests that the 17 estimates are not independent quantities (e.g., they share a σ_0 value and are based on an identical object), and the rms dispersion of 5.3 Mpc is an uncertainty related to the wavelength and the adopted FP relation parameters for each measurement. Therefore, we consider a typical intrinsic scatter in the FP relation along $\log(r_{\rm eff})$ of 0.09 dex (23% of the value) as our distance error. Considering these factors, we adopt $37.7 \pm 8.7\ h_{70}^{-1}$ Mpc as the FP-based distance. Note that this is an angular diameter distance, and at $z = 0.009783$ of NGC 4993 (Levan et al. 2017), the luminosity distance is 2% larger at $38.4 \pm 8.9\ h_{70}^{-1}$ Mpc. We also note that the mean angular diameter distance of 37.7 Mpc is accurate to about $5.3\ \mathrm{Mpc}/\sqrt{17} = 1.3$ Mpc in regard to uncertainties due to wavelengths and FP parameter sets.

[9] Wegner et al. (2003) listed a value within a 0.595 h_{100}^{-1} kpc radius aperture, and this value is converted to the value for an aperture with 1/8 of $r_{\rm eff}$ using Equation (1) of Cappellari et al. (2006).

Table 2
Host Galaxy Property from SED Fitting

	t (Gyr)	τ (Gyr)	M_* ($M_\odot$)	$E(B-V)$	$\mathrm{SFR}_{100\,\mathrm{Myr}}$ ($M_\odot\,\mathrm{yr}^{-1}$)	Z
Best-fit	6.5	0.5	3.80e+10	0.000	4.1e–3	0.02
2nd best-fit	4.25	0.3	2.93e+10	0.025	1.9e–3	0.02
10 Gyr model	10.0	0.5	5.48e+10	0.075	8.7e–6	0.008
Piovan	12.0	⋯	⋯	0.025	0.0	0.008

Table 3
FP Distance to NGC 4993

Filter	Distance (Mpc)	Mean Distance (Mpc)
B	31.7[a], 34.7[b], 36.4[c], 41.7[d]	36.1 (4.2)
V	31.8[a], 33.0[e], 32.3[f], 41.8[d]	34.7 (4.7)
R	36.2[a], 41.3[d]	38.8 (3.6)
I	36.9[a], 44.6[g], 46.9[d]	42.8 (5.2)
J	38.8[a]	38.8
H	39.6[a]	39.6
K	44.1[a], 28.4[h]	36.3 (11.1)
Average	37.7 (5.3)	38.2 (2.7)

Notes. The numbers in parentheses are the rms scatter of the corresponding quantities, not errors of the values. The FP parameters are adjusted so that σ_0 is the value inside an aperture radius of $\frac{1}{8}\,r_{\rm eff}$.
[a] La Barbera et al. (2010).
[b] Bender et al. (1998).
[c] de la Rosa et al. (2001).
[d] Bernardi et al. (2003).
[e] D'Onofrio et al. (2008).
[f] Jun & Im (2008).
[g] Scodeggio et al. (1997).
[h] Pahre et al. (1998).

6. Discussion

Structural parameters suggest that NGC 4993 is an ordinary elliptical galaxy, having an SB profile consistent with that of a bulge-dominated galaxy with $n \sim 4$ and sitting right in the middle of the size–mass relation of local early-type galaxies (Yoon et al. 2017). The disk-like features and the dust lanes, common in post-merger ellipticals (e.g., Shabala et al. 2012; Kim & Im 2013) suggest that NGC 4993 has gone through merging activities before. Indeed, this galaxy has been noted in the past as a "shell elliptical" (Carter et al. 1988).

One can derive the dynamical mass ($M_{\rm dyn}$) of NGC 4993 and see how it compares with the mean stellar mass. Using the relation of $M_{\rm dyn} = 5\,r_{\rm eff}\,\sigma_{\rm eff}^2/{\rm G}$ (Cappellari et al. 2006), where $\sigma_{\rm eff}$ is the σ within an aperture with $r_{\rm eff}$, and rescaling σ_0 to $\sigma_{\rm eff}$ with Equation (1) of Cappellari et al. (2006), we get $M_{\rm dyn} = (5.2\text{–}7.8) \times 10^{10}\,M_\odot$ for $r_{\rm eff} = 3$ kpc. The value becomes smaller if we adopt $r_{\rm eff} = 2$ kpc in the near-infrared. These values are in good agreement with the mean stellar mass. The properties of NGC 4993 are consistent with some of the short GRB host galaxies, although our age estimate of $\gtrsim$3 Gyr lies at the old end. The trace of a minor merging event suggests that the BNS system might have come from the merged galaxy. Another possible explanation for the BNS from a galaxy with a very old stellar population is the dynamical origin (Bae et al. 2014) where the NS binaries can be formed within globular clusters via three body processes and eventually undergo merger after they get kicked out of the cluster.

We find that the location of GW170817 is only about $10\farcs23 \pm 0\farcs08$ ($\sim$2 kpc) away from the center of NGC 4993, or 2/3 to 1 of $r_{\rm eff}$ in projected distance. Short GRBs tend to occur at outer regions of host galaxies (a median offset of 1.5 $r_{\rm eff}$; Fong & Berger 2013). So far, about 25% of short GRBs have been found at a projected offset of $<r_{\rm eff}$ from the host galaxy center (Troja et al. 2008; Fong & Berger 2013; Li et al. 2016), so the occurrence of the event near the center is not very unusual.

The luminosity distance of 38.4 ± 8.9 Mpc agrees with the distance estimate from the GW signal (40^{+8}_{-14} Mpc; Abbott et al. 2017b) as well as the previous estimate to the group distance ($\sim$40 Mpc; Sakai et al. 2000). This independent assessment of the distance can possibly improve constraints on the GW source property such as the inclination of the binaries and eventually masses and spins.

This work was supported by the National Research Foundation (NRF) grant Nos. 2017R1A3A3001362 and 2016R1D1A1B03934815, funded by the Korea government (MSIT). H.M.L. was supported by the NRF grant No. NRF-2016R1D1A1A02937544. C.U.L. and S.L.K. were supported by the KASI grant 2017-1-830-03. This research has made use of the KMTNet system operated by KASI, and the data were obtained at three host sites of CTIO, SAAO, and SSO. We thank the staffs of iTelescope.Net and the KMTNet sites for their excellent support.

Facilities: *HST*(ACS), AAVSO, Pan-STARRS, *GALEX*, *WISE*, 2MASS.

ORCID iDs

Myungshin Im https://orcid.org/0000-0002-8537-6714
Jongwan Ko https://orcid.org/0000-0002-9434-5936

References

Abbott, B. P., Abbott, R., Abbott, T. D., et al. 2016, PhRvX, 6, 041015
Abbott, B. P., Abbott, R., Abbott, T. D., et al. 2017a, PhRvL, 118, 221101
Abbott, B. P., Abbott, R., Abbott, T. D., et al. 2017b, PhRvL, 119, 161101
Bae, Y. B., Kim, C., & Lee, H. M. 2014, MNRAS, 440, 2714
Bender, R., Saglia, R. P., Ziegler, B., et al. 1998, ApJ, 493, 529
Berger, E. 2014, ARA&A, 52, 43
Bernardi, M., Sheth, R. K., Annis, J., et al. 2003, AJ, 125, 1866
Beuing, J., Bender, R., Mendes de Oliveira, C., Thomas, D., & Maraston, C. 2002, A&A, 395, 431
Bruzual, G., & Charlot, S. 2003, MNRAS, 344, 1000
Cappellari, M., Bacon, R., Bureau, M., et al. 2006, MNRAS, 366, 1126
Capperllari, M., McDermid, R. M., Alatalo, K., et al. 2012, Natur, 484, 485
Carter, D., Prieur, J. L., Wilkinson, A., Sparks, W. B., & Malin, D. F. 1988, MNRAS, 235, 813
Chabrier, G. 2003, PASP, 115, 763
Chambers, K. C., Magnier, E. A., Metcalfe, N., et al. 2016, arXiv:1612.05560
Choi, C., & Im, M. 2017, JKAS, 50, 71
Coutler, D. A., Kilpatrick, C. D., Siebert, M. R., et al. 2017, Sci, https://doi.org/10.1126/science.aap9811
de la Rosa, I. G., de Carvalho, R. R., & Zepf, S. 2001, AJ, 122, 93
D'Onofrio, M., Fasano, G., Varela, J., et al. 2008, ApJ, 685, 875
Fitzpatrick, E. L. 1999, PASP, 111, 63

Fong, W., & Berger, E. 2013, ApJ, 776, 18
Goldstein, A., Veres, P., Burns, E., et al. 2017, ApJL, 848, L14
Im, M., Choi, C., & Kim, K. 2015, JKAS, 48, 207
Jun, H., & Im, M. 2008, ApJL, 678, L97
Kim, D., & Im, M. 2013, ApJ, 766, 109
Kim, S.-L., Lee, C.-U., Park, B.-G., et al. 2016, JKAS, 49, 37
Ko, J., Im, M., & Lee, H. M. 2012, ApJ, 745, 181
La Barbera, F., de Carvalho, R. R., de la Rosa, I. G., & Lopes, P. A. A. 2010, MNRAS, 408, 1335
Lee, S.-K., Im, M., Kim, J.-W., et al. 2015, ApJ, 810, 90
Leibler, C. N., & Berger, E. 2010, ApJ, 725, 1202
Levan, A. J., Lyman, J. D., Tanvir, N. R., et al. 2017, ApJL, 848, L28
Li, Y., Zhang, B., & Lu, H.-J. 2016, ApJS, 227, 7
Metzger, B. D. 2017, LRR, 20, 3
Michałowski, M. J., Kamble, A., Hjorth, J., et al. 2012, ApJ, 755, 85
Ogando, R. L. C., Maia, M. A. G., Pellegrini, P. S., & da Costa, L. N. 2008, AJ, 135, 2424
Pahre, M., Djorgovski, S. G., & de Carvalho, R. R. 1998, AJ, 116, 1591
Peng, C. Y., Ho, L. C., Impey, C. D., & Rix, H.-W. 2010, AJ, 139, 2097
Piovan, L., Tantalo, R., & Chiosi, C. 2003, A&A, 408, 559
Riess, A., Macri, L. M., Hoffmann, S. L., et al. 2016, ApJ, 826, 56
Sakai, S., Mould, J. R., Hugnes, S. M. G., et al. 2000, ApJ, 529, 698
Savchenko, V., Ferrigno, C., Kuulkers, E., et al. 2017, ApJL, 848, L15
Schlafly, E. F., & Finkbeiner, D. P. 2011, ApJ, 737, 103
Scodeggio, M., Giovanelli, R., & Haynes, M. P. 1997, AJ, 113, 101
Shabala, S. S., Ting, Y.-S., Kaviraj, S., et al. 2012, MNRAS, 423, 59
Shim, H., Im, M., Lee, H. M., et al. 2011, ApJ, 727, 14
Troja, E., King, A. R., O'Brien, P. T., Lyons, N., & Cusumano, G. 2008, MNRAS, 385, L10
Troja, E., Piro, L., van Eerten, H., et al. 2017, Natur, https://doi.org/10.1038/nature24290
Troja, E., Sakamoto, T., Cenko, S. B., et al. 2016, ApJ, 827, 10
Wegner, G, Bernardi, M., Willmer, C. N. A., et al. 2003, AJ, 126, 2268
Yoon, Y., Im, M., & Kim, J.-W. 2017, ApJ, 834, 73